coatings

MDPI

Communication

Predicting New Single/Multiphase-Structure High-Entropy Alloys Using a Pattern Recognition Network

Fang Wang [1], Jiahao Wang [1], Jiayu Wang [2,*], Ruirui Wu [1,3] and Ke Liu [1,*]

[1] School of Materials Science and Engineering, Taiyuan University of Science and Technology, Taiyuan 030024, China; 2001044@tyust.edu.cn (F.W.); 18306877898@163.com (J.W.)
[2] School of Materials Science and Engineering, Harbin Institute of Technology (Shenzhen), Shenzhen 518055, China
[3] Shanxi Taigang Stainless Steel Precision Strip Co., Ltd., Taiyuan 030006, China
* Correspondence: 23b355003@stu.hit.edu.cn (J.W.); liuke@tyust.edu.cn (K.L.); Tel.: +86-135-1616-5971 (J.W.); +86-183-3515-0716 (K.L.)

Abstract: Machine learning methods were employed to predict the phase structures of high-entropy alloys (HEAs). These alloys were classified into four categories: bcc (body-centered cubic), fcc (face-centered cubic), bcc+fcc (body-centered cubic and face-centered cubic) and others (containing intermetallic compounds and other structural alloys). The utilized algorithm was a Pattern Recognition Network (PRN) utilizing cross-entropy as the loss function, enabling the prediction of HEAs' phase formation probability. The PRN algorithm demonstrated an accuracy exceeding 87% based on the test data. The PRN algorithm successfully predicted the transformation from fcc to fcc+bcc and subsequently to a bcc structure with the increase in Al content in AlxCoCu6Ni6Fe6 and AlxCoCrCuNiFe HEAs. In addition, AlxCoCu6Ni6Fe6 (x = 1, 3, 6, 9) HEAs were prepared using a vacuum arc furnace, and the microstructure of the as-cast alloy was tested by means of XRD, SEM, and EBSD, confirming the high consistency between the predicted and observed phase structures. This study showcases the efficacy of the PRN algorithm in predicting both single- and multiphase-structure high-entropy alloys, offering valuable insights into alloy design and development.

Keywords: machine learning; high-entropy alloys; phase structure; model prediction

Citation: Wang, F.; Wang, J.; Wang, J.; Wu, R.; Liu, K. Predicting New Single/Multiphase-Structure High-Entropy Alloys Using a Pattern Recognition Network. *Coatings* **2024**, *14*, 690. https://doi.org/10.3390/coatings14060690

Academic Editor: Hideyuki Murakami

Received: 11 April 2024
Revised: 27 May 2024
Accepted: 28 May 2024
Published: 1 June 2024

1. Introduction

High-entropy alloys (HEAs) have garnered increasing attention due to their exceptional mechanical and functional properties, encompassing high wear resistance, strength, hardness, radiation resistance, and biocompatibility [1]. Originally, HEAs were developed to craft multi-principal simple solid solution alloys with high mixed entropy, aiming to achieve multiphase structures capable of meeting diverse performance requirements through the adjustment of each principal element's composition ratios [2,3]. The vast elemental and compositional space of HEAs poses challenges in identifying novel alloys with distinct phases [3]. Recent reports highlighted CoCrFeMnNi HEAs with an fcc structure, showcasing outstanding damage tolerance with fracture toughness exceeding 200 MPa $m^{1/2}$, surpassing that of pure metals, polymers, and metallic glasses. Additionally, these alloys exhibit enhanced mechanical properties at cryogenic temperatures. Investigations by Senkov et al. [4] explored the microstructure evolution and compressive flow behavior of refractory HEAs with a bcc structure, illustrating alloy yield stress stabilization above 600 °C, indicative of superior thermal stability compared to conventional superalloys. Wani et al. [5] synthesized AlCoCrNiFe2.1 eutectic HEAs with dual-phase structures of fcc (L12) and bcc (B2), showcasing satisfactory strength–ductility combinations. Recent research underscores the significance of identifying bcc, fcc, bcc+fcc, and other phases for future HEA applications, such as hydrogen storage, metallic biomaterials, and structural materials [4–10]. Hence, rational alloying element selection and crystal structure design

are imperative to cater to diverse property requirements. Determining the composition space of HEAs with different structures (bcc, fcc, bcc+fcc, etc.) is challenging due to the complex interactions among multi-principle elements, often resulting in crystal structures differing from individual elements [1]. Recent studies have employed thermodynamic empirical parameters, pseudo-binary strategies, first-principle density functional theory, and CALPHAD-aided predictions to forecast HEA phase formation, albeit at significant experimental and computational costs [11–14].

Machine learning (ML) has emerged as an efficient data processing method capable of uncovering underlying data patterns and reducing experimental and simulation expenses. The abundance of experimental HEA data enables ML algorithms to predict phase formation across wide composition spaces. Zhang Lei et al. [15] employed three algorithms—multilayer perceptron, support vector machine, and gradient boosting decision tree—to predict HEA phase formation based on a dataset of 407 alloys. Jaiswal et al. [16] utilized seven algorithms, including logistic regression, support vector machine, and artificial neural networks, for HEA phase formation prediction. Jiang et al. [17] established a property-oriented artificial neural network model to rapidly discover novel aluminum alloys with comprehensive mechanical properties. Krishna et al. [18] utilized six machine learning algorithms to predict solid solutions and intermetallic multi-phase mixtures, with artificial neural networks yielding the highest prediction accuracy of 80.5%. Although various ML algorithms have been applied, the differences in accuracy are minimal, suggesting insignificant variation in HEA phase prediction. Furthermore, there is a lack of ML algorithms predicting HEA phase formation probability [15,16,18]. Hence, the adoption of the Pattern Recognition Network (PRN) with high prediction accuracy and probability is warranted. Based on phase formation criteria from the literature, thermodynamic empirical parameters—such as enthalpy of mixing (ΔHmix) [19], valence electronic concentration (VEC) [20], entropy of mixing (ΔSmix) [21], difference in atomic sizes (δ) [21], Ω parameter [21], and Φ parameter [22]—along with their value ranges are proposed for HEA formation prediction.

In this study, we aimed to predict HEA phase structures utilizing the PRN algorithm with cross-entropy as the loss function, facilitating phase formation probability prediction. The algorithm's predictive performance for new compositions was experimentally validated. HEA data from various groups (bcc, fcc, bcc+fcc, and other alloys) were analyzed by combining parameters like VEC, Tm, δ, ΔHmix, and ΔSmix.

2. Materials and Methods

The PRN algorithm consists of an input layer, a hidden layer, an output layer, and a softmax layer, and each layer is fully connected. The PRN algorithm is given as follows:

$$O_j = \varphi(x)\left(\sum_{i=1}^{n} w_i x_i + \theta_j\right) \quad (1)$$

$$y = \frac{e^{o_i}}{\sum_{j=1}^{n} e^{o_j}} \quad (2)$$

where x_i is the input, w_i is the weights, θ_j is the thresholds, and O_j is the output. $\varphi(x)$ is the active function; for the hidden layer, $\varphi(x) = \frac{2}{1+e^{-2*x}} - 1$, and $\varphi(x) = x$ for the output layer. Formula (2) is the active function of the softmax layer, which converts the network output into probability results.

The calculated design parameters and collected phase structure data [23–25] underwent statistical analysis utilizing the Pandas module [16,18]. Figure 1a illustrates the pairwise correlation of design parameters, with the diagonal line representing the density plot of all parameters in the study. The diagonal depicts the distribution density of design parameters, highlighting the need to consider all parameters for the PRN algorithm. A heat map, generated using the Pearson correlation coefficient, illustrates the interdependence of design parameters across different phase structures. The heat map, depicted in Figure 1b,

displays both negative and positive correlations between parameters, with values ranging from −0.69 to 0.35, indicating varying degrees of correlation. For instance, ΔHmix and δ exhibit a positive correlation, indicating that an increase in ΔHmix results in a larger δ. Conversely, the negative correlation coefficient between Tm and VEC suggests that an increase in Tm leads to a decrease in VEC, consistent with observations from the paired plot. Figure 1c, plotted using Plotly in Python, presents a parallel coordinate diagram of phase formation, showcasing the variation in design parameters and confirming the overlapping boundary between bcc, fcc, bcc+fcc, and other phases.

The prediction of HEAs with bcc, fcc, bcc+fcc, and other phase structures was conducted using the PRN algorithm, formulated and implemented in MATLAB. The model utilized training data to predict phase formation for new alloy groups, leveraging insights gained through the training algorithm. In this study, 70% of the dataset was randomly allocated for training, while 15% was used for validation and 15% was used for testing purposes. Experimental validation was conducted to verify the predictive performance of the algorithm for new compositions.

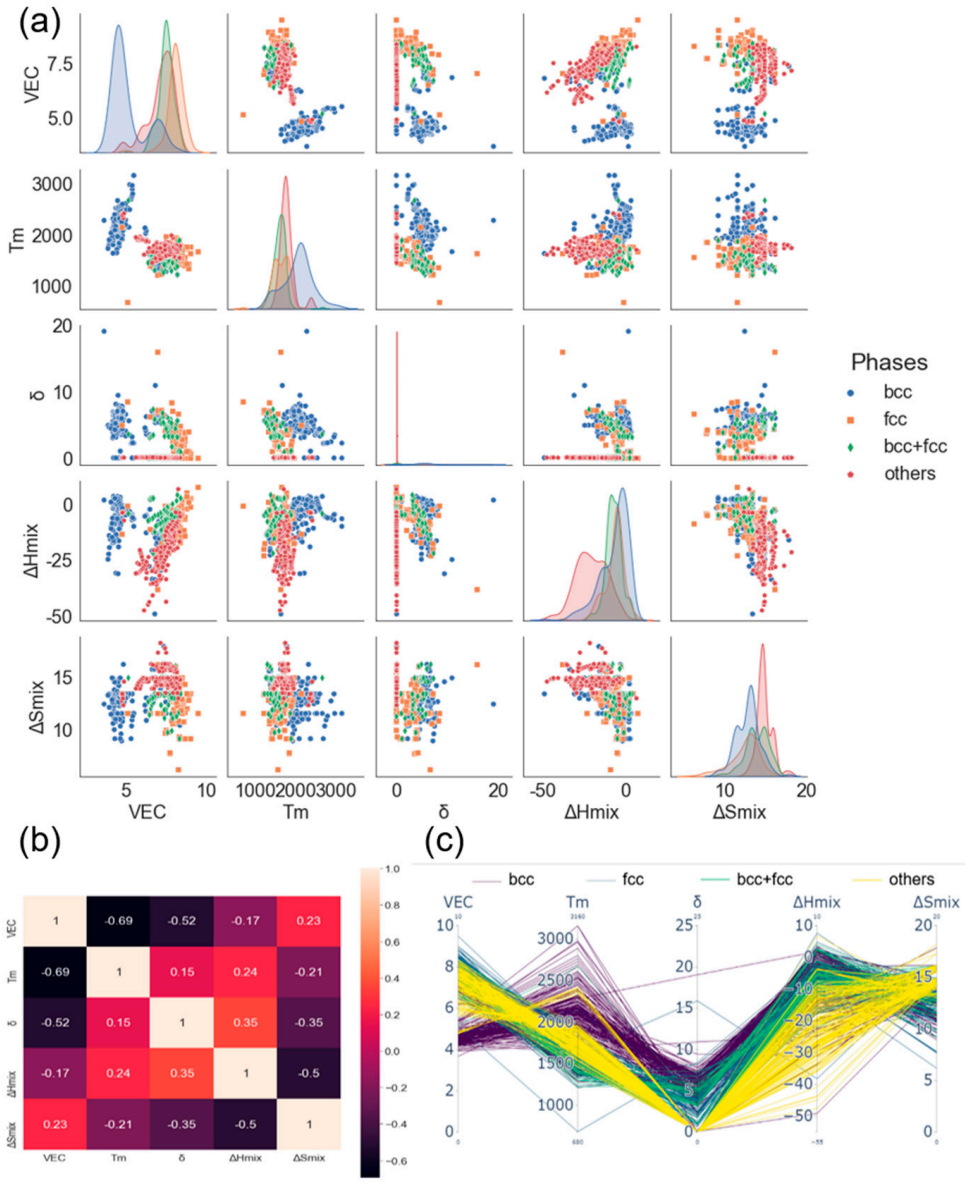

Figure 1. (**a**) Pair plot for design parameters used for HEA prediction. (**b**) Heatmap for total studied dataset. (**c**) Parallel coordinate plot for the total studied data with phases.

3. Results and Discussion

Artificial neutral networks are the most widely used models to predict material properties and structures, accelerating the discovery of new materials with excellent performance. Lee et al. [26] identified phase information of HEAs using a deep neural network (multilayer neural network). Zheng et al. [27] utilized an artificial neural model to predict the γ' phase volume fraction and yield strength of HEAs. Dixit et al. [28] used an artificial neutral model to predict eight coexisting phases in HEAs. Mi et al. [29] developed high-performance and low-cost magnesium alloys using an artificial neutral network model. Wu et al. [30] employed an artificial neutral network model to develop an affordable new Ti alloy with bone-like modulus. The PRN algorithm employed in this study is a supervised learning algorithm utilizing cross-entropy as the loss function. Each data point utilized for training possesses a target label, with weights and thresholds optimized through the backpropagation algorithm to achieve the required training set accuracy for accurate classification of new components. It has been demonstrated that a single hidden layer can effectively approximate most non-linear functions [31,32]. Hence, a single hidden layer is adopted in the PRN algorithm, with the number of nodes in the hidden layer significantly impacting PRN accuracy. A small number of nodes in the hidden layer may compromise generalization ability, while an excessive number can prolong training time and increase the risk of overfitting. To determine the optimal hyperparameter of the PRN algorithm, the number of nodes in the hidden layer was varied from 2 to 10, and the prediction accuracy of the test data was assessed, as depicted in Figure 2. The results reveal that the PRN algorithm achieves optimal prediction accuracy with eight nodes in the hidden layer. The training process of the PRN algorithm is illustrated in Figure 3a, showing that after 40 epochs, the validation performance reached its peak value of 0.090554. Figure 3b displays the error instances during the training process.

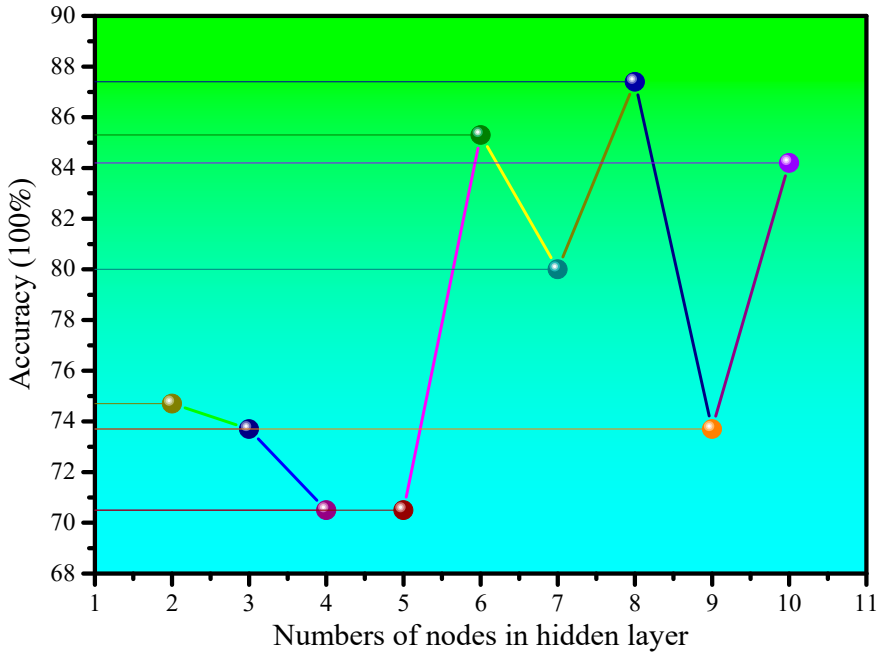

Figure 2. PRN algorithm performance with different nodes numbers in hidden layer.

The confusion matrix serves as a metric for assessing the performance of the PRN algorithm by comparing predicted and experimental results [26]. Each column of the confusion matrix represents predicted outcomes, while each row represents experimental outcomes. Higher values along the diagonal indicate greater prediction accuracy. Figure 3c illustrates the confusion matrix generated by the PRN algorithm for classifying bcc, fcc, bcc+fcc, and other categories. The matrix encompasses data from 634 compositions, comprising 444 training samples, 95 validation samples, and 95 testing samples. The graph

presents normalized actual and predicted phase values, with correct classifications depicted along the diagonal. Notably, the PRN achieves prediction accuracies exceeding 85% for the training, validation, testing, and overall datasets, surpassing values reported in the literature [15,16,18,23]. Specifically, the PRN algorithm achieves 93.3% accuracy for bcc data, 84.6% for fcc data, 75% for bcc+fcc data, and 90.6% for other data. The PRN algorithm demonstrates a high accuracy of 87.4% based on the test dataset. Furthermore, varying the number of hidden layer neurons can enhance PRN prediction accuracy on the test data, underscoring its potential to expedite the discovery of new components.

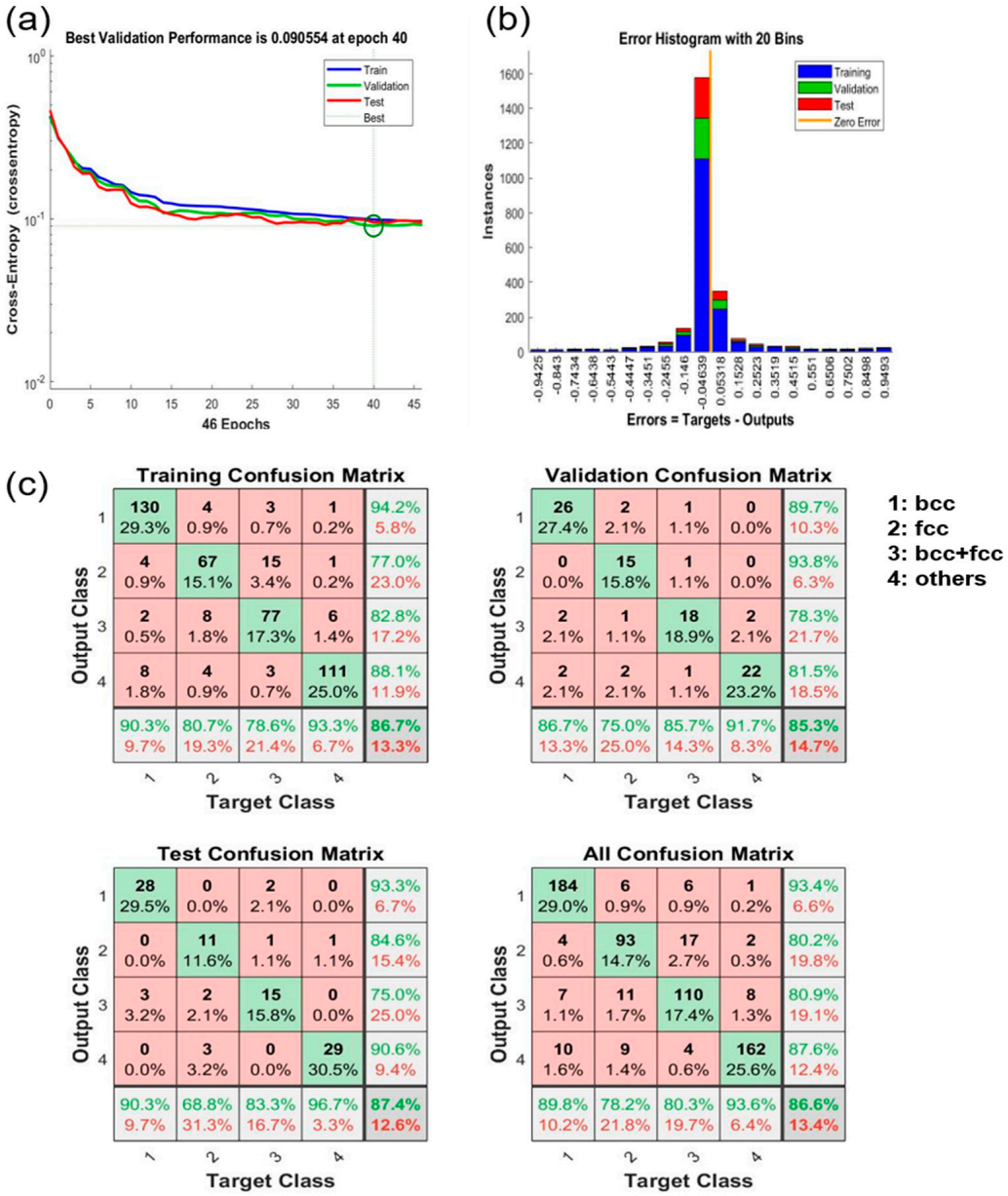

Figure 3. Results from the PRN. (**a**) Cross entropy with epochs. (**b**) Error histogram. (**c**) Confusion matrix of training, validation, testing, and all datasets.

AlxCoCu6Ni6Fe6 HEAs were prepared using a vacuum arc furnace, with melting repeated five times to ensure chemical homogeneity. Rigaku Ultima IV X-ray diffraction (XRD) analysis employing Cu Kα radiation was utilized to verify the phase structure. Samples were scanned over a 2θ range from 20° to 90° at a scan speed of 5° min^{-1}. The microstructure of specimens was characterized using the Crossbeam 350 SEM equipped with an EBSD probe running at 20 kV, and the EBSD samples were prepared using vibration

polishing. Figure 4 presents the XRD patterns of the newly developed alloys. From Figure 4, it can be seen that the Al6CoCu6Ni6Fe6 alloy has diffraction peaks with both bcc and fcc structures. The Al1CoCu6Ni6Fe6 and Al3CoCu6Ni6Fe6 alloys only have diffraction peaks with fcc structures, while Al9CoCu6Ni6Fe6 only has diffraction peaks with bcc structures. Among them, peaks of a partially ordered bcc phase (B2) were also observed in the Al6CoCu6Ni6 and Al9CoCu6Ni6 alloys [33,34]. Considering that the ordered bcc phase and disordered bcc phase belong to the body-centered-cubic system, the datasets used for the training pattern network (PRN) pre-classified both the ordered bcc structure and disordered bcc structure into the bcc category. It can be further observed from Figure 4 that the Al6CoCu6Ni6Fe6 HEA has (100) diffraction peaks at 32 degrees, indicating that the bcc structure of Al6CoCu6Ni6Fe6 is composed of an ordered B2 phase and a disordered bcc phase. The same applies to the Al9CoCu6Ni6Fe6 alloy.

To further examine the microstructural morphology and phase structure of AlxCoCu6Ni6Fe6 HEAs, EBSD observation was conducted, as shown in Figure 5. Figure 5a–d depict the EBSD band contrast maps of AlxCoCu6Ni6Fe6 (x = 1, 3, 6, 9) HEAs. It can be seen from Figure 5e–h that the phase structures of AlxCoCu6Ni6Fe6 (x = 1, 3, 6, 9) were fcc, fcc, bcc+fcc and bcc, respectively, which is consistent with the XRD results. Table 1 provides statistics on HEA composition, predicted results, and experimental results. The PRN algorithm successfully predicts the transition from fcc to fcc+bcc and then to a bcc structure with increasing Al content in AlxCoCu6Ni6Fe6 and AlxCoCrCuNiFe HEAs, with exceptions noted for certain compositions, as shown in the bold font in the Table 1. This discrepancy is attributed to overlapping design parameters of bcc and bcc+fcc, as depicted in Figure 6. The PRN algorithm effectively elucidates the influence of aluminum on HEAs' crystal structure and offers a probabilistic explanation for prediction errors. This study offers valuable insights for the design of HEAs with desired phase structures.

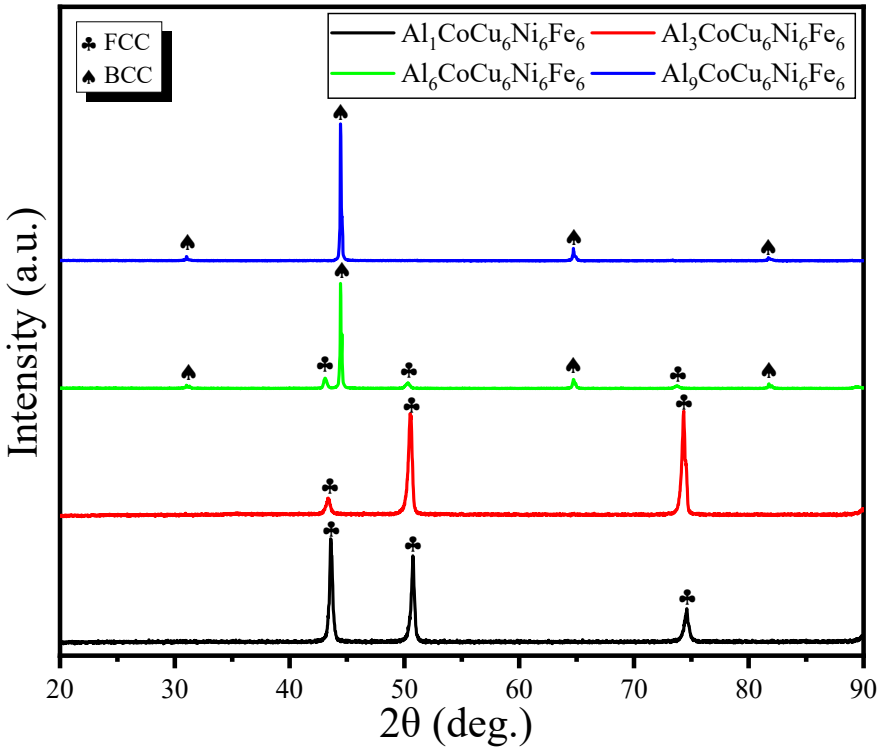

Figure 4. XRD diagram of experimental results of the aluminum $Al_xCoCu_6Ni_6Fe_6$ system.

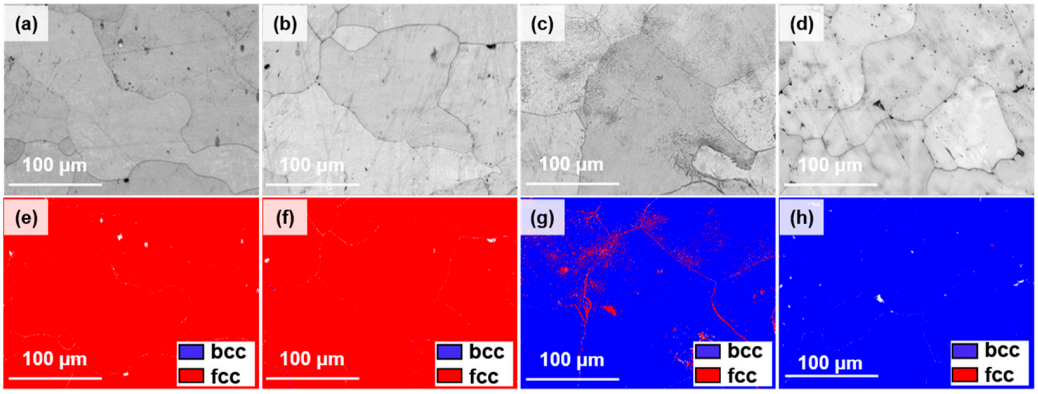

Figure 5. (**a**–**d**) Band contrast maps of AlxCoCu6Ni6Fe6 (x = 1, 3, 6, 9) HEAs. (**e**–**h**) Phase maps of AlxCoCu6Ni6Fe6 (x = 1, 3, 6, 9) HEAs.

Table 1. Prediction probability of single/multiphase-structure high-entropy alloys using the PRN algorithm.

Composition	bcc	fcc	bcc+fcc	Others	Predict	Experiment	Reference
Al1CoCu6Ni6Fe6	0	0.96	0.04	0	fcc	fcc	This work
Al3CoCu6Ni6Fe6	0	0.87	0.12	0.01	fcc	fcc	This work
Al6CoCu6Ni6Fe6	0.01	0.42	0.56	0.01	bcc+fcc	bcc+fcc	This Work
Al9CoCu6Ni6Fe6	**0.01**	**0.13**	**0.86**	**0**	**bcc+fcc**	**bcc**	**This Work**
Al0CoCrCuNiFe	0.01	0.89	0.08	0.02	fcc	fcc	[35]
Al0.3CoCrCuNiFe	0.02	0.58	0.33	0.07	fcc	fcc	[35]
Al0.5CoCrCuNiFe	**0.02**	**0.33**	**0.54**	**0.11**	**bcc+fcc**	**fcc**	**[35]**
Al0.8CoCrCuNiFe	0.02	0.11	0.73	0.13	bcc+fcc	bcc+fcc	[35]
Al1CoCrCuNiFe	0.02	0.06	0.80	0.12	bcc+fcc	bcc+fcc	[35]
Al1.3CoCrCuNiFe	0.02	0.02	0.86	0.10	bcc+fcc	bcc+fcc	[35]
Al1.5CoCrCuNiFe	0.02	0.01	0.89	0.08	bcc+fcc	bcc+fcc	[35]
Al1.8CoCrCuNiFe	0.02	0.01	0.91	0.06	bcc+fcc	bcc+fcc	[35]
Al2CoCrCuNiFe	0.01	0.01	0.93	0.05	bcc+fcc	bcc+fcc	[35]
Al2.3CoCrCuNiFe	0.01	0.01	0.94	0.04	bcc+fcc	bcc+fcc	[35]
Al2.5CoCrCuNiFe	0.01	0.01	0.95	0.03	bcc+fcc	bcc+fcc	[35]
Al2.8CoCrCuNiFe	**0.01**	**0**	**0.96**	**0.03**	**bcc+fcc**	**bcc**	**[35]**
Al3CoCrCuNiFe	**0.01**	**0.01**	**0.96**	**0.02**	**bcc+fcc**	**bcc**	**[35]**

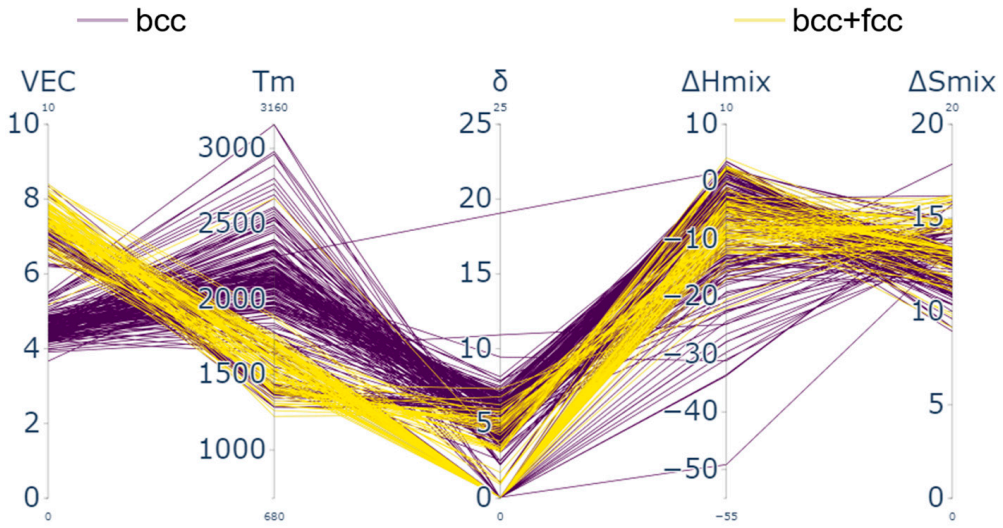

Figure 6. Parallel coordinate plot of bcc- and bcc+fcc-structure high-entropy alloys.

4. Conclusions

In this study, AlxCoCu6Ni6Fe6 high-entropy alloys (HEAs) were formulated to investigate the influence of aluminum content on crystal structure, guided by predictions from the PRN algorithm regarding HEAs' phase structures. As the Al content increased, the crystal structure transitioned from fcc to fcc+bcc and subsequently to bcc. Furthermore, the PRN algorithm offered novel insights into predicting failures resulting from comparable prediction probabilities associated with different structures. The data-driven approach employed in this investigation holds promise for structural prediction in diverse material systems, thus expediting the discovery of novel materials.

Author Contributions: F.W.: Conceptualization, Methodology, Software, Validation, Formal analysis, Investigation, Data Curation, Writing—Original Draft, Writing—Review and Editing, Funding acquisition. J.W. (Jiahao Wang): Data Curation, Supervision, Formal analysis. J.W. (Jiayu Wang): Writing—Review and Editing, Supervision, Funding acquisition. R.W.: Microscopic characterization, Data Curation. K.L.: Writing—Review and Editing, Supervision, Funding acquisition. All authors have read and agreed to the published version of the manuscript.

Funding: The authors gratefully acknowledge the financial support from the National Natural Science Foundation of China (U23A20628, Provided by Fang Wang), the Taiyuan University of Science and Technology Scientific Research Initial Funding (20232095, Provided by Ke Liu) and Excellent Dr. Laijin Research Funding (20242006, Provided by Ke Liu).

Institutional Review Board Statement: Not applicable.

Informed Consent Statement: Not applicable.

Data Availability Statement: The data used in the current study are available from the corresponding author based on reasonable request.

Conflicts of Interest: Author Ruirui Wu was employed by Shanxi Taigang Stainless Steel Precision Strip Co., Ltd. The remaining authors declare that the research was conducted in the absence of any commercial or financial relationships that could be construed as a potential conflict of interest.

References

1. Miracle, D.B.; Senkov, O.N. A critical review of high entropy alloys and related concepts. *Acta Mater.* **2017**, *122*, 448–511. [CrossRef]
2. Senkov, O.N.; Miller, J.D.; Miracle, D.B.; Woodward, C. Accelerated exploration of multi-principal element alloys with solid solution phases. *Nat. Commun.* **2015**, *6*, 6529. [CrossRef] [PubMed]
3. Li, Z.; Pradeep, K.G.; Deng, Y.; Raabe, D.; Tasan, C.C. Metastable high-entropy dual-phase alloys overcome the strength–ductility trade-off. *Nature* **2016**, *534*, 227–230. [CrossRef]
4. Senkov, O.N.; Wilks, G.B.; Scott, J.M.; Miracle, D.B. Mechanical properties of nbmotaw and vnbmotaw refractory high entropy alloys. *Intermetallics* **2011**, *19*, 698–706. [CrossRef]
5. Wani, I.S.; Bhattacharjee, T.; Sheikh, S.; Lu, Y.P.; Chatterjee, S.; Bhattacharjee, P.P.; Guo, S.; Tsuji, N. Ultrafine-grained alcocrfeni2.1 eutectic high-entropy alloy. *Mater. Res. Lett.* **2016**, *4*, 174–179. [CrossRef]
6. Gludovatz, B.; Hohenwarter, A.; Catoor, D.; Chang, E.H.; George, E.P.; Ritchie, R.O. A fracture-resistant high-entropy alloy for cryogenic applications. *Science* **2014**, *345*, 1153–1158. [CrossRef]
7. Liu, K.; Wang, J.Y.; Li, X.; Qin, Q.; Wu, S.J.; Yu, H.C. A new lightweight Al2.7TiVCrCu high entropy alloy with excellent strength and toughness after homogenization treatment. *Mater. Sci. Eng. A* **2023**, *869*, 144779. [CrossRef]
8. Todai, M.; Nagase, T.; Hori, T.; Matsugaki, A.; Sekita, A.; Nakano, T. Novel tinbtazrmo high-entropy alloys for metallic biomaterials. *Scr. Mater.* **2017**, *129*, 65–68. [CrossRef]
9. Hori, T.; Nagase, T.; Todai, M.; Matsugaki, A.; Nakano, T. Development of non-equiatomic Ti-Nb-Ta-Zr-Mo high-entropy alloys for metallic biomaterials. *Scr. Mater.* **2019**, *172*, 83–87. [CrossRef]
10. Liu, K.; Li, X.; Wang, J.Y.; Zhang, Y.; Guo, X.; Wu, S.J.; Yu, H.C. Investigation of mechanical and corrosion properties of light and high hardness cast AlTiVCrCu0.4 high entropy alloy. *Mater. Charact.* **2023**, *200*, 112878. [CrossRef]
11. Jiang, H.; Han, K.; Gao, X.; Lu, Y.; Cao, Z.; Gao, M.C.; Hawk, J.A.; Li, T.J. A new strategy to design eutectic high-entropy alloys using simple mixture method. *Mater. Des.* **2018**, *142*, 101–105. [CrossRef]
12. Jin, X.; Zhou, Y.; Zhang, L.; Du, X.; Li, B.S. A new pseudo binary strategy to design eutectic high entropy alloys using mixing enthalpy and valence electron concentration. *Mater. Des.* **2018**, *143*, 49–55. [CrossRef]

13. Saboktakin, R.M.; Minouei, H.; Lee, B.J.; Toroghinejad, M.R.; Hong, S.I. Effects of carbon and molybdenum on the nanostructural evolution and strength/ductility trade-off in Fe40Mn40Co10Cr10 high-entropy alloys. *J. Alloys Compd.* **2022**, *911*, 165108. [CrossRef]
14. Rahul, M.R.; Phanikumar, G. Design of a Seven-Component Eutectic High-Entropy Alloy. *Metall. Mater. Trans. A* **2019**, *50*, 2594–2598. [CrossRef]
15. Zhang, L.; Cai, H.; Liu, J.; Ouyang, Y.F.; Peng, Q.; Du, Y. Machine learning reveals the importance of the formation enthalpy and atom-size difference in forming phases of high entropy alloys. *Mater. Des.* **2020**, *193*, 108835. [CrossRef]
16. Jaiswal, U.K.; Krishna, Y.V.; Rahul, M.R.; Phanikumar, G. Machine learning-enabled identification of new medium to high entropy alloys with solid solution phases. *Comput. Mater. Sci.* **2021**, *197*, 110623. [CrossRef]
17. Jiang, L.; Wang, C.S.; Fu, H.D.; Shen, J.; Zhang, Z.H.; Xie, J.X. Discovery of aluminum alloys with ultra-strength and high-toughness via a property-oriented design strategy. *J. Mater. Sci. Technol.* **2022**, *98*, 33–43. [CrossRef]
18. Yegi, V.K.; Ujjawal, K.J.; Rahul, M.R. Machine learning approach to predict new multiphase high entropy alloys. *Scr. Mater.* **2021**, *197*, 113804.
19. Zhang, Y.; Zhou, Y.J.; Lin, J.P.; Chen, G.L.; Liaw, P.K. Solid-Solution Phase Formation Rules for Multi-component Alloys. *Adv. Eng. Mater.* **2008**, *10*, 534–538. [CrossRef]
20. Guo, S.; Ng, C.; Lu, J.; Liu, C.T. Effect of valence electron concentration on stability of fcc or bcc phase in high entropy alloys. *J. Appl. Phys.* **2011**, *109*, 103505. [CrossRef]
21. Yang, X.; Zhang, Y. Prediction of high-entropy stabilized solid-solution in multi-component alloys. *Mater. Chem. Phys.* **2012**, *132*, 233–238. [CrossRef]
22. Ye, Y.F.; Wang, Q.; Lu, J.; Liu, C.T.; Yang, Y. Design of high entropy alloys: A single-parameter thermodynamic rule. *Scr. Mater.* **2015**, *104*, 53–55. [CrossRef]
23. Li, Y.; Guo, W.L. Machine-learning model for predicting phase formations of high-entropy alloys. *Phys. Rev. Mater.* **2019**, *3*, 095005. [CrossRef]
24. Machaka, R. Machine Learning Based Prediction of Phases in High-Entropy Alloys. *Comput. Mater. Sci.* **2020**, *188*, 110244. [CrossRef]
25. Gorsse, S.; Nguyen, M.H.; Senkov, O.N.; Miracle, D.B. Database on the mechanical properties of high entropy alloys and complex concentrated alloys. *Data Brief* **2018**, *21*, 2664–2678. [CrossRef] [PubMed]
26. Lee, S.Y.; Byeon, S.; Kim, H.S.; Jin, H.; Lee, S. Deep learning-based phase prediction of high-entropy alloys: Optimization, generation, and explanation. *Mater. Des.* **2021**, *197*, 109260. [CrossRef]
27. Zheng, T.; Hu, X.B.; He, F.; Wu, Q.F.; Han, B.; Da, C.; Li, J.J.; Wang, Z.J.; Wang, J.C.; Kai, J.; et al. Tailoring nanoprecipitates for ultra-strong high-entropy alloys via machine learning and prestrain aging. *J. Mater. Sci. Technol.* **2021**, *69*, 156–167. [CrossRef]
28. Dixit, S.; Singhal, V.; Agarwal, A.; Rao, A.K.P. Multi-label phase-prediction in high-entropy-alloys using Artificial-Neural-Network. *Mater. Lett.* **2020**, *268*, 127606. [CrossRef]
29. Mi, X.X.; Tian, L.J.; Tang, A.; Kang, J.; Peng, P.; She, J.; Wang, H.L.; Chen, X.H.; Pan, F.S. A reverse design model for high-performance and low-cost magnesium alloys by machine learning. *Comput. Mater. Sci.* **2022**, *201*, 110881. [CrossRef]
30. Wu, C.T.; Chang, H.T.; Wu, C.Y.; Chen, S.W.; Huang, S.Y.; Huang, M.M.; Pan, Y.T.; Bradbury, P.; Chou, J.; Yen, H.W. Machine learning recommends affordable new Ti alloy with bone-like modulus. *Mater. Today* **2020**, *34*, 41–50. [CrossRef]
31. Prieto, A.; Prieto, B.; Ortigosa, E.M.; Ros, E.; Pelayo, F.; Ortega, J.; Rojas, I. Neural networks: An overview of early research, current frameworks and new challenges. *Neurocomputing* **2016**, *214*, 242–268. [CrossRef]
32. Basheer, I.A.; Hajmeer, M.; Microbiol, J. Artificial neural networks: Fundamentals, computing, design, and application. *J. Microbiol. Methods* **2000**, *43*, 3–31. [CrossRef] [PubMed]
33. Praveen, S.; Murty, B.S.; Kottada Ravi, S. Alloying behavior in multi-component AlCoCrCuFe and NiCoCrCuFe high entropy alloys. *Mater. Sci. Eng. A* **2012**, *534*, 83–89. [CrossRef]
34. Ma, Y.; Wang, Q.; Jiang, B.B.; Li, C.L.; Hao, J.M.; Li, X.N.; Dong, C.; Nieh, T.G. Controlled formation of coherent cuboidal nanoprecipitates in body-centered cubic high-entropy alloys based on $Al_2(Ni,Co,Fe,Cr)_{14}$ compositions. *Acta Mater.* **2018**, *147*, 213–225. [CrossRef]
35. Yeh, J.W.; Chen, S.K.; Lin, S.J.; Gan, J.Y.; Chin, T.S.; Shun, T.T.; Tsau, C.H.; Chang, S.Y. Nanostructured High-Entropy Alloys with Multiple Principal Elements: Novel Alloy Design Concepts and Outcomes. *Adv. Eng. Mater.* **2004**, *6*, 299–303. [CrossRef]